

# Electronic Supplementary Material

## Fluoride ions adsorption from water by CaCO<sub>3</sub> enhanced Mn-Fe mixed metal oxides

Xinyuan Wang<sup>1</sup>, Heriberto Pfeiffer<sup>2</sup>, Jiangjiang Wei<sup>1</sup>, Jinyu Wang (✉)<sup>1</sup>, Jinli Zhang (✉)<sup>1,3</sup>

<sup>1</sup> School of Chemistry and Chemical Engineering/Key Laboratory for Green Processing of Chemical Engineering of Xinjiang Bingtuan, Shihezi University, Shihezi 83200, China

<sup>2</sup> Instituto de Investigaciones en Materiales, Universidad Nacional Autónoma de México, Cd. Universitaria, Del. Coyoacán, CP 04510 Ciudad de México, Mexico

<sup>3</sup> School of Chemical Engineering and Technology, Tianjin University, Tianjin 300350, China

E-mails: wjy0993@126.com (Wang J); zhangjinli@tju.edu.cn (Zhang J)

### TEXT S1

After the synthesis processes, the MFC and CMFC samples were characterized by X-ray diffraction (XRD), scanning electron microscopy (SEM) and N<sub>2</sub> adsorption-desorption techniques, as well as using infrared (FTIR) and X-ray photoelectron (XPS) spectroscopies. Initially, the crystal phases present on each sample were determined by powder XRD, using a Bruker AXS, D8 Advance, equipment, with a Cu K radiation ( $\lambda=1.5406 \text{ \AA}$ ). The SEM morphological and elemental distribution analyses were performed on a Hitachi S4800 equipment, adapted with an X-Flash EDX Detector 5010. Additionally, the microstructural characterization was complemented by the specific surface area and pore volume using the Brunauer-Emmett-Teller (BET) and Barrett-Joyner-Halenda (BJH) models respectively, from the N<sub>2</sub> adsorption-desorption measurements performed on a Micromeritics, ASAP 2460 apparatus. The FTIR spectra of the samples were recorded in the 4000 to 400 cm<sup>-1</sup> range on a spectrometer Agilent Cary 630, by using pressed KBr-containing sample pellets. The XPS was obtained on a Thermo Fisher Scientific K-Alpha using Al K $\alpha$  radiation. The binding energy of all the elements were calibrated relative to the carbon impurity presence (C<sub>1s</sub> at 284.8 eV).

## TEXT S2

After the complete characterization process, the fluoride adsorption experiments were performed as follows. Sodium fluoride (NaF, Titan Discovery, 0.221 g) was dissolved in ultrapure water to prepare a fluoride solution with precise concentration (100 mg/L). All the fluoride adsorption experiments were performed in a constant temperature oscillator, maintained at 200 rpm and reaction time of 24 hours, to ensure the equilibrium of reaction. The reacted solution was filtered through by 0.22  $\mu\text{m}$  nylon filter membrane, and the residual fluoride concentration in the solution was measured using a fluoride ion selective electrode (PF-02). The batch adsorption method was used to explore adsorption process on the surface of CMFC sample. The following method was used to calculate adsorption capacity ( $q_e$ ) and removal efficiency ( $R_e$ ):

$$q_e = (C_0 - C_e) \times V/m \quad (1)$$

$$R_e(\%) = 100(C_0 - C_e)/C_0 \quad (2)$$

In the equations 1 and 2,  $C_0$  represents the fluoride concentration of the solution to be adsorbed, and  $C_e$  is the equilibrium adsorption concentration (mg/L). Dosage of the adsorbent is represented by  $m$  (g), and the volume of the solution is  $V$  (L).

In the adsorption process, the isotherm Langmuir adsorption model can be defined as:

$$C_e/q_e = C_e/q_{max} + 1/K_L q_{max} \quad (3)$$

while, Freundlich adsorption isotherm model is:

$$\log(q_e) = \log(K_F) + \log(C_e)/n \quad (4)$$

where,  $K_L$  and  $K_F$  are the Langmuir and Freundlich constants, respectively. Also,  $n$  is a Freundlich index related to adsorption strength,  $C_e$  (mg/L) is the adsorption equilibrium concentration of fluoride, and  $q_e$  is the adsorption capacity (mg/g) of fluoride by the adsorbent when the system is in equilibrium.

In the dynamics experiment, the kinetic expressions for the adsorption models can be described as follows:

Pseudo-first-order kinetics;

$$\log(q_e - q_t) = \log - k_1 t \quad (5)$$

Pseudo-second-order kinetics;

$$1/(q_e - q_t) = k_2 t + 1/q_e \quad (6)$$

where,  $k_1$  and  $k_2$  are the rate constants of the pseudo-first-order kinetics, pseudo-second-order kinetics, respectively;  $t$  is the contact time;  $C$  is the thickness of the liquid film.  $q_e$  and  $q_t$  are the fluoride adsorption capacities (mg/g) at system equilibrium and at time  $t$ , respectively.

## Text S3

Three unique regions with different morphologies in Fig. S3a were analyzed using Raman spectra. As shown in Fig. S3b, Site A has a rod-like structure, corresponding to the red curve in the Raman spectra, of which the Raman shift at 1085  $\text{cm}^{-1}$  is the symmetrical vibration of  $\text{CaCO}_3$ . The Raman shifts at 717  $\text{cm}^{-1}$  and 284  $\text{cm}^{-1}$  is respectively due to the in-plane bending mode and vibrational lattice mode of carbonate [21-23]. Thus the rod-like structure corresponds to the  $\text{CaCO}_3$  crystal in MFC. Site B is nano-granular structure, blue curve in Raman spectra, which also have the in-plane bending mode and vibrational lattice mode of carbonate (711  $\text{cm}^{-1}$  and 284  $\text{cm}^{-1}$ ) [21, 24], except of the characteristic Raman frequency shift at 649  $\text{cm}^{-1}$ , which is typical of  $\text{MnCO}_3$  crystals[25, 26]. Site C is lamellar structure, green curve in Raman spectra, of which the peak at 658  $\text{cm}^{-1}$  is ascribed to the disorder within the  $\alpha\text{-Fe}_2\text{O}_3$  crystal [27,28]. However, according to EDS results (Fig. S3c and Fig. S3d), MFC has a good uniform distribution of elements O, Fe, Ca and Mn. It is reasonable to conclude that the uniform distribution of these elements is caused by the high dispersion of the above unique regions on the surface.

MFC is obtained by uniform precipitation of mixed metal nitrate solution through hydrothermal reaction, with urea as the uniform precipitator in this process. First, the urea molecules begin to hydrolyze, producing stable hydroxide and carbonate ions, the key components of the morphological transition. As the hydrothermal reaction time increased, urea hydrolysis resulted in uniform release of hydroxyl groups, and the pH of the solution increased, preventing the occurrence of partial supersaturation and facilitating uniform nucleation[29]. Due to the different properties of metal ions, the order of precipitation is slightly different. According to  $K_{sp}$  (solubility product constant) calculation, the precipitation sequence is  $\text{Fe}(\text{OH})_3 > \text{CaCO}_3 > \text{MnCO}_3$  during hydrothermal process [30]. Nanocrystals have high surface energy and are easy to aggregate. Initially formed nanoparticles are the basic components of the precursor. To minimize surface energy, primary particles cluster together to produce larger particles [31]. Hydrothermal reaction is carried out at high temperature, and the growth rate of crystal is accelerated with the acceleration of nuclear proliferation. Afterward, numerous nanosheets tended to form a three-dimensional intercalation structure by a self-assembly process to minimize the surface energy of the reaction system. Finally, the crystallinity gradually increased and reached a maximum degree through the Ostwald-ripening process [32]. However, some particles fail to fuse with the main core and become dispersed and fine nanoparticles distributed on the surface of the main block. This is the main reason for the surface morphology of Fig.2 (a3).

**Table S1** The error associated to the specific surface area of MFC and CMFC.

$S_{\text{BET}} / \text{m}^2 \cdot \text{g}^{-1}$	Test 1	Test 2	Test 3	Average	Standard deviation
MFC	11.9	9.3	10.9	10.7	1.31
CMFC	20.3	14.8	16.7	17.3	2.79

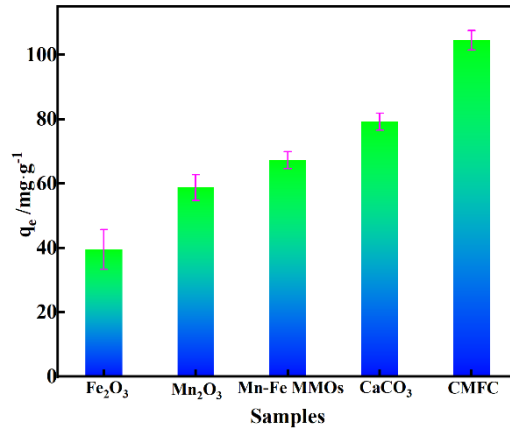


Fig. S1 Single component and CMFC adsorption capacity.

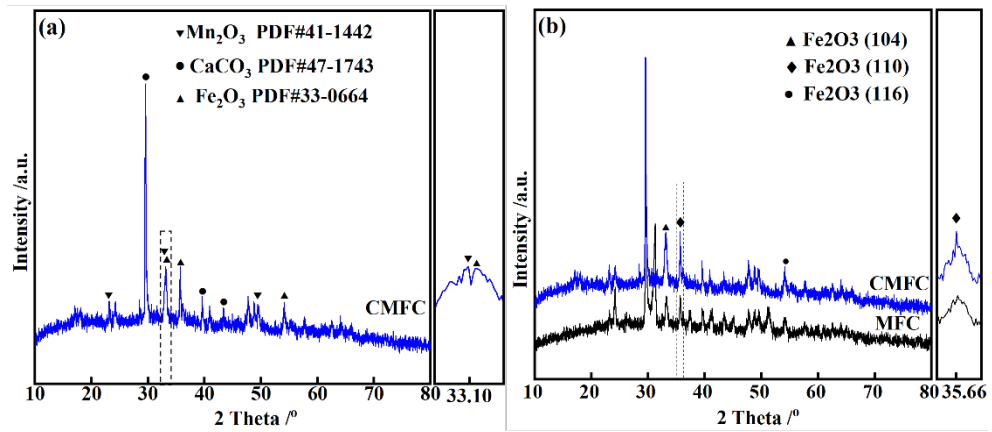


Fig. S2 Magnified local diffraction peak of crystal plane of  $\text{Fe}_2\text{O}_3$  (110) (a); Local magnification of XRD pattern of CMFC around  $31.10^\circ$ .

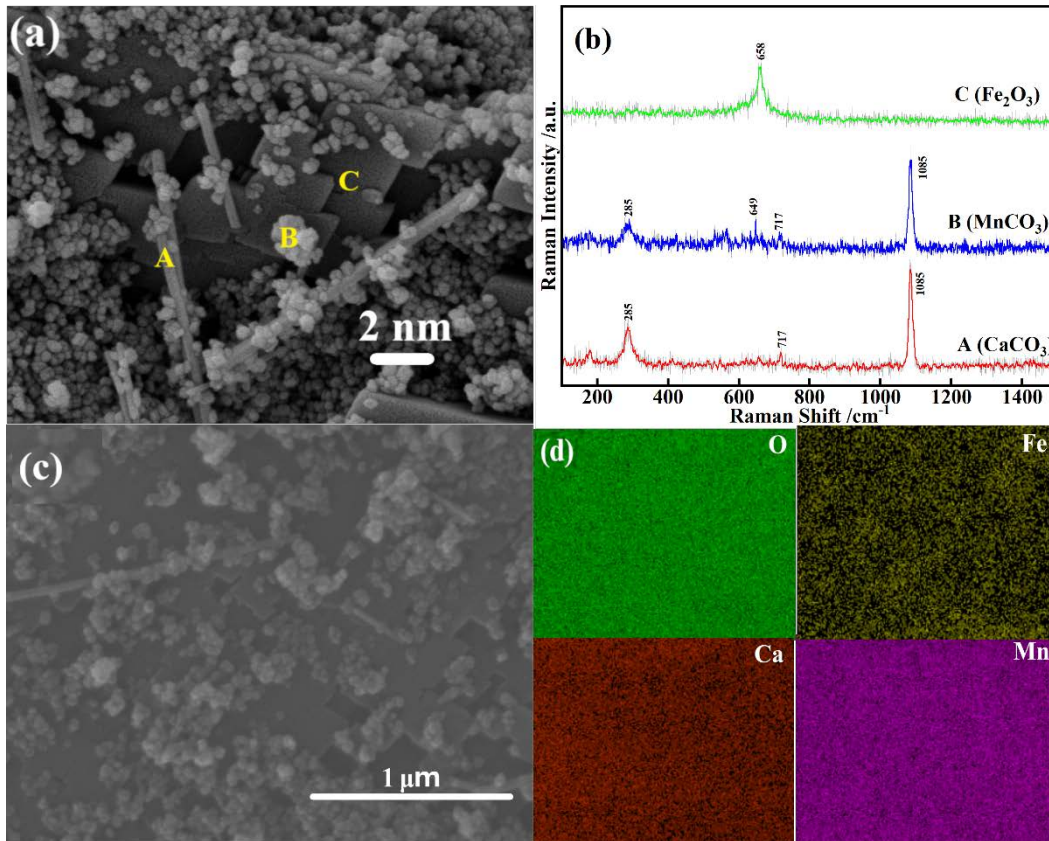


Fig. S3 SEM image of MFC (a); Raman pattern of MFC (b); EDS Mapping of MFC (c) and (d).

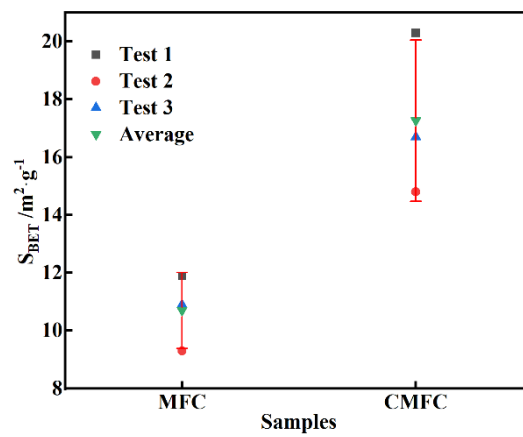


Fig. S4 The error associated to the specific surface area of MFC and CMFC.